LAWRENCE
LIVERMORE
NATIONAL
LABORATORY

LLNL-CONF-870318

Simulating Energy Localization of Millimeter-Scale Defects In HMX Due To Sub-Shock Loading

H. K. Springer

October 7, 2024

17th International Detonation Symposium
Kansas City, MO, United States
August 5, 2024 through August 9, 2024

Disclaimer

Simulating Energy Localization of Millimeter-Scale Defects in HMX Due To Sub-Shock Loading

H. Keo Springer, J. E. Reaugh

Lawrence Livermore National Laboratory
Livermore, CA 94550

Abstract. The exposure of explosives to harsh loading environments can cause premature ignition in millimeter-scale defects. In order to improve our understanding of explosive survivability in sub-shock environments ($P \leq 1$ GPa), we perform multi-physics simulations to determine how changes to defect geometry, material properties, and loading conditions influence energy localization mechanisms in HMX. We explore different energy localization mechanisms such as plastic work heating and defect gas compression with thermal conduction to the adjacent explosive. Our defect-focused simulations consider millimeter-scale spherical and ellipsoidal pores. Pores are filled with air. We apply a triangular loading pulse with peak pressures of 100-1000 MPa and 1-4 millisecond duration. The competition of adiabatic gas compression and plasticity-viscous mechanisms are discussed. Insights from our simulation-based studies provide the basis for developing new explosive safety models and refining strategies for improving explosive survivability to avoid catastrophic consequences.

Introduction

Dynamic, sub-shock loading of explosives can cause premature ignition at millimeter-scale defects and catastrophic consequences[1]. Bowden & Yoffe suggested that rapid collapse of a gas pocket, friction processes and heating by viscous flow are viable ignition mechanisms for explosives subjected to sub-shock dynamic loading[2]. Millimeter-scale bubbles of argon (γ = 1.67) are found to be more effective at promoting reactions in nitromethane than butane (γ = 1.1) which demonstrates the importance of gas compression and gas type in ignitions[3]. Mader simulated these experiments in some of the earliest numerical studies of pore collapse in explosives and showed that voids promote hot spot mechanisms and build up to initiation[4-7]. Starkenberg demonstrated the importance of adiabatic compression of gas adjacent to the explosive in order to accelerate its ignition. They showed that gas pressurization rate and gas layer thickness govern explosive ignition. However, this study employed ideal gas P-V response and did not use realistic equation of state properties for the air which can alter its compression and heating[8]. Additional theoretical pore collapse studies focused on the heating due to plastic work in a thin shell of material around the collapsing cavities[9-10]. Frey considered shear banding mechanisms as means of producing hotspots in explosives whereby the thermal softening exceeds the strain and strain-rate hardening[11-12]. More recent numerical studies have demonstrated the importance of crystal level mechanical processes on strain localization and shear banding which contribute to hot spot mechanisms[13-15]; however, these studies and similar studies have not considered large defects at the millimeter scale.

For the present study, we simulate heating and hot spot formation in mm-scale pore defects in HMX subjected to sub-shock loading conditions. We investigate how the pore shape (spherical, ellipsoidal), HMX material properties (anisotropic elastic response based on crystal structure, magnitude of yield strength), air properties (realistic equation of state) and loading conditions (triangular pulse with 100-1000 MPa peaks and 1-4 millisecond pulsewidth) influence heating of the solid explosive from plastic work heating and thermal conduction from the compressed gas.

HMX Material Model

Elasticity

In our simulations, we employ either an isotropic or anisotropic elasticity model. For anisotropic elasticity, the Generalized Hooke's Law linearly relates stress and strain, $\sigma_{ij} = C_{ijkl}\varepsilon_{ij}$ where the elasticity tensor has the symmetries $C_{ijkl} = C_{ijlk} = C_{klij}$ and hence has 21 independent components. For the deviatoric stress, this can be expressed incrementally as,

$$\Delta\tau_{ij} = \left(C_{ijkl} - \frac{1}{3}\delta_{ij}C_{mnkl}\right) d_{kl}\Delta t + \frac{1}{3}\left(C_{ijkk} - \frac{1}{3}\delta_{ij}C_{mmkk}\right)\frac{\dot{v}}{v}\Delta t$$

Anisotropic elastic moduli coefficients are shown in Table 1.

Table 1. Elastic moduli[13]. All values in GPa.

C_{11}	C_{22}	C_{33}	C_{44}	C_{55}	C_{66}	
22.2	23.9	23.4	9.2	11.1	10.1	
C_{12}	C_{13}	C_{23}	C_{15}	C_{25}	C_{35}	C_{46}
9.6	13.2	13.0	0.1	-4.7	-1.6	-2.5

Plasticity

Since yield stress is varied in our studies to bound values in the appropriate pressure-strain rate regime, we use a simple perfectly plastic model with a von Mises yield criterion. Yield strength values are 25 and 100 MPa, respectively. These yield strength values bound HMX strength for the applied loading conditions and associated strain-rates (100/s-1000/s).

Unreacted EOS

A simplified form of the Murnaghan EOS is used for our studies where the loading pressures does not exceed 1 GPa,

$$P = \frac{K}{n}\left[\left(\frac{1}{v}\right)^{n} - 1\right]$$

where K is the bulk modulus, n is the derivative dK/dP, and v is the relative volume. Table 2 shows the model parameters.

Table 2. Murnaghan EOS Parameters

K	21.0	GPa
n	4.48	Unitless

Heat Capacity & Thermal Conductivity

Table 3 shows temperature-dependent heat capacity and thermal conductivity data for HMX. The data is used in tables that can be interpolated.

Table 3. HMX heat capacity and thermal conductivity[16].

T	HC (cal/g-K)	k (cal/cm-g-K)
298 K	0.24	1.28×10^{-3}
373 K	0.30	1.09×10^{-3}
433 K	0.34	1.02×10^{-3}
563 K	0.40	8.15×10^{-4}
623 K	0.46	7.50×10^{-4}
>=773 K	0.55	1.0×10^{-4}

Air Material Model

For the air initially at ambient conditions, we employ a tabular EOS with temperature-dependent thermal conductivity and heat capacity. The tabular EOS is Livermore EOS (LEOS) number 2264.

ALE3D Simulation Details

Two dimensional, axisymmetric sub-shock simulations are performed in the multi-physics code, ALE3D[17]. Triangular loading with 1 or 4 millisecond pulsewidths and 100, 500, or 1000 Mpa peak pressures are applied to simulation domain. See Figure 1. One (1) mm diameter spherical pores and 3:1 aspect ratio ellipsoidal pores are considered. Ellipsoidal pores have volume equal to that of the spherical pores and are oriented in the direction of loading or perpendicular to loading direction. Pores are either filled with air or unfilled (vacuum). When the anisotropic elastic model is used, HMX crystal orientations are (110) or (010) planes in the $P2_1/n$ space group consistent with previous experimental studies[13]. The domain in these simulations is 5 mm x 5 mm which represents an upper bound of HMX crystal size. The mesh resolution is 0.01 mm.

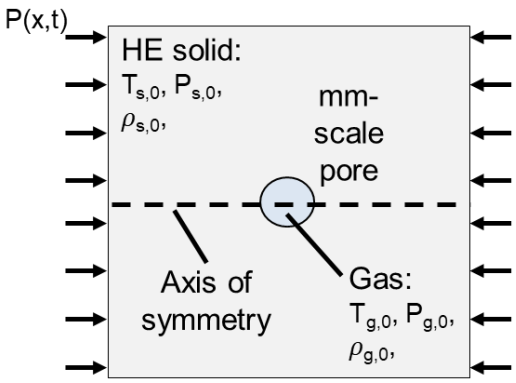

Figure 1. Schematic of ALE3D Simulations

Results

Baseline Simulation

Figure 2 shows the normalized pore volume, $V_{pore}(t)/V_{pore,0}$ (current pore volume divided by the initial pore volume), normalized air temperature in the pore, $T_g(t)/T_{g,0}$ (average air temperature divided by the initial air temperature of 298 K), and the normalized peak temperature in the solid HE, $T_s(t)/T_{s,0}$ (current temperature of HE adjacent to pore divided by the initial HE temperature of 298 K) for a 1 mm diameter spherical pore filled with air that is subjected to a triangular pulse with peak pressure, P_{peak} = 1 GPa and pulsewidth, t_{pulse} = 1 ms. The yield strength, Y_0 = 100 MPa.

Figure 2a shows that after initial yielding in the solid HE around the pore, it collapses and the pore volume decreases to nearly 0.001 of its initial volume. Fringe plots of equivalent plastic strain (EPS) show the extent of plastic work in the solid as the pore collapses. The pore volume doesn't significantly increase after the loading phase is completed. Plastic strain in the adjacent solid HE prevents re-expansion of the pore and is responsible for the irreversible pore collapse.

Figure 2b shows the $T_g(t)/T_{g,0}$ predicted by simulation which can exceed 6. Also shown are comparisons to a gamma law gas model for air (γ = 1.4) and gamma law gas model fit to the results of simulation (γ = 1.3). The large discrepancy between the predictions and the gamma law gas is due the large gas compression in this loading scenario. Figure 2c shows the $T_s(t)/T_{s,0}$ adjacent to the collapsing pore which consists of plastic work and conduction from the hot air.

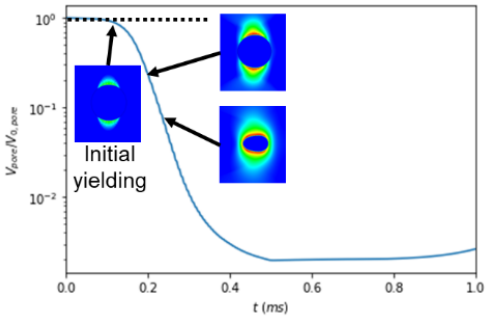

a)

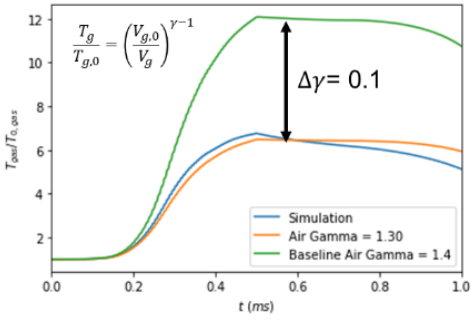

b)

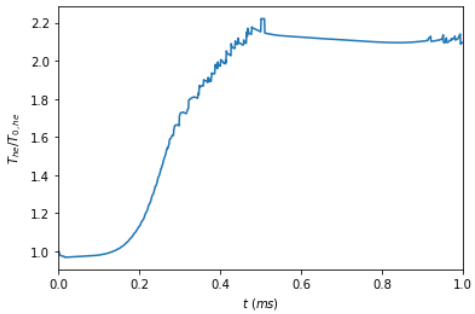

c)

Figure 2. a) normalized pore volume, $V_{pore}(t)/V_{pore,0}$, b) normalized air temperature in the pore, $T_g(t)/T_{g,0}$, and the c) normalized peak temperature in the solid HE, $T_s(t)/T_{s,0}$.

Effects of Thermal Coupling

Figure 3a shows the effects of thermal conduction on $T_s(t)/T_{s,0}$ for a 1 mm diameter spherical pore filled with air that is subjected to a triangular pulse with P_{peak} = 1 GPa and t_{pulse} = 4 ms. The yield strength, Y_0 = 100 MPa. Conduction is active in the "thermal" case and inactive in the "no thermal" case. The solid temperature is significantly higher in the thermal case because the hot, compressed air is allowed to conduct heat to the adjacent HE. In the no thermal case, heating in the solid is due to plastic work alone with no contributions from the hot gas. Figure 3b loading is identical to Figure 3a with the exception that P_{peak} = 250 MPa. The lower peak pressure relative to the yield strength reduces the adiabatic compression of the gas and there's less heating by via thermal conduction, i.e., lower P_{peak}/Y_0 yields lower air temperatures thus reduced heating of solid HE. The peak compression ($V_{pore,peak}/V_{pore,0}$) for the 1 GPa loading case is ~0.0025 and for the 250 MPa loading case it is ~0.08. Altogether, adiabatic gas compression can add significant heating to HE over plastic work alone which increases the propensity for ignition.

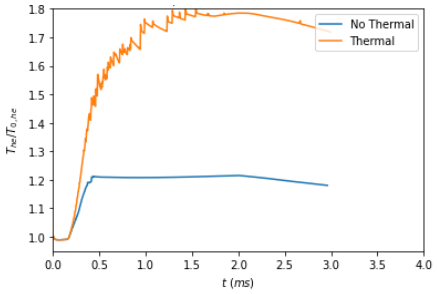

a)

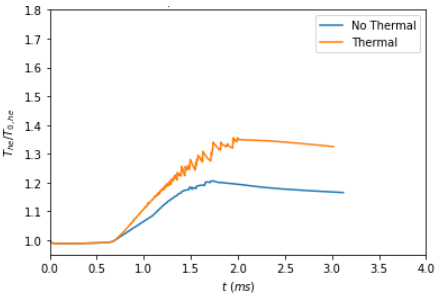

b)

Figure 3. The effects of thermal conduction on $T_s(t)/T_{s,0}$ for a 1 mm diameter spherical pore filled with air that is subjected to a triangular pulse with pulsewidth, t_{pulse} = 4 ms and a) P_{peak} = 1 GPa, b) P_{peak} = 250 MPa. Y_0 = 100 MPa.

Effects of Pore Shape

Figure 4 shows the effects pore shape on $T_s(t)/T_{s,0}$. One mm diameter spherical pore and 3:1 aspect ratio ellipsoidal pores filled with air are simulated. Ellipsoidal pores have volume equal to that of the spherical pores and are oriented in the direction of loading (prolate ellipsoid) or perpendicular to loading direction (oblate ellipsoid). Domain is subjected to a triangular pulse with peak pressure, P_{peak} = 1 GPa and pulsewidth, t_{pulse} = 4 ms. The yield strength, Y_0 = 25 MPa. We observed the highest solid temperatures in the spherical pore case with prolate and oblate ellipsoidal pores yielding relatively lower temperatures. This is in contrast to higher shock pressure scenarios where where the prolate ellipsoids yield the highest solid temperatures due in part to enhanced hydrodynamic jetting[18]. The more uniform pore collapse without hydrodynamic jetting is believed

to be responsible for the differences observed in these non-shock scenario.

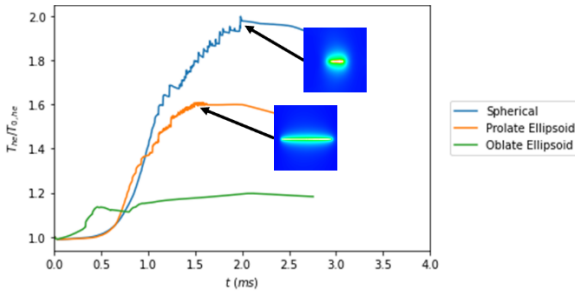

Figure 4. The effects of pore shape on $T_s(t)/T_{s,0}$ for the case of a 1 mm diameter spherical pore, prolate ellipsoid, and oblate ellipsoid. triangular pulse with peak pressure, P_{peak} = 1 GPa and pulsewidth, t_{pulse} = 4 ms. The yield strength, Y_0 = 25 MPa.

Effects of Crystal Orientation

Figure 5 shows the effects of HMX crystal orientation on $T_s(t)/T_{s,0}$ when using the anisotropic elastic model. HMX crystal orientations are (110) and (010) planes in the $P2_1/n$ space group consistent with previous experimental studies[19]. Results of the isotropic model is shown for comparison. In this case, we perform 2D plane strain simulations of a 1 mm diameter pore filled with air that is subjected to a triangular pulse with P_{peak} = 500 MPa and t_{pulse} = 1 ms. Y_0 = 100 MPa. There are small differences (~10%) in $T_s(t)/T_{s,0}$ between the (010) and (110) crystal orientations; however, the morphology of the collapsing pores can be quite different.

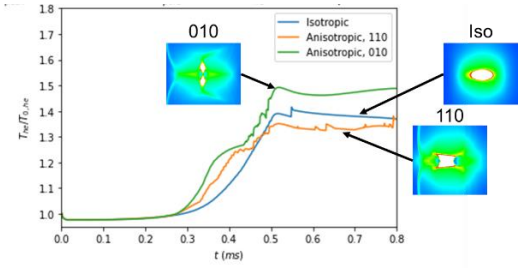

Figure 5. $T_s(t)/T_{s,0}$ for crystal orientations (110) and (010) planes in the $P2_1/n$ space group. Results of the isotropic model is shown for comparison. 2D plane strain simulations of a 1 mm diameter pore filled with air that is subjected to a triangular pulse with P_{peak} = 500 MPa and t_{pulse} = 1 ms. Y_0 = 100 MPa.

Conclusions

The temperature of the pore gas (air) can increase significantly during non-shock loading scenarios where $T_g(t)/T_{g,0}$ can exceed 6. Air temperature increases with increasing P_{peak}/Y_0. $T_{g,0}\left(\frac{V_{g,0}}{V_g}\right)^{\gamma-1}$ does an adequate job of representing the air temperature with an adjusted value for γ.

Studies on thermal conduction show that heating of the HE by the hot air can be significant and augments HE heating by plastic work. Solid HE heating is more sensitive to pore shape than to crystal orientation.

In some cases, the pore volume doesn't significantly increase after the loading phase is completed. Plastic strain in the adjacent solid HE prevents re-expansion of the pore and is responsible for the irreversible pore collapse.

Overall, these studies are important to develop and enhance macroscale models of explosive safety, such as the HERMES model[20] and the ViscoSCRAM model[21].

Acknowledgment

This work was performed under the auspices of the U.S. Department of Energy by Lawrence Livermore National Laboratory under Contract DE-AC52-07NA27344 and was supported by the LLNL-LDRD Program under Project No. 24-SI-004. LLNL-CONF-870318.

References

1. S. Swaszek, E.L. Baker, Proceedings of the IMEMTS Conference, 2019.
2. F. P. Bowden, A. D. Yoffe, *Ignition and Growth of Explosions in Liquids and Solids*, Cambridge Univ. Press, 1952.
3. A. W. Campbell, W. C. Davis, J. R. Travis; *Phys. Fluids* 1 April 1961; 4 (4): 498–510.
4. C. L. Mader, *Phys. Fluids* 1963; 6 (3): 375–381.
5. C. L. Mader; Los Alamos Scientific Report LA-3077 1964.

6. C. L. Mader; *Phys. Fluids* 1965; 8 (10): 1811–1816.
7. C. L. Mader; Los Alamos Scientific Report LA-3325 1965.
8. J. Starkenberg, in 7th International Detonation Symposium (ONR, Annapolis, MD, 1981), pp. 3-16.
9. M. Carroll and A. Holt, J. Appl. Phys. 1972, 43(4), 1626–1636.
10. B. Khasainov, A. Attetkov, and A. Borisov, Khim. Fiz. 1996, 15(7), 53–125.
11. R. B. Frey, in 7th International Detonation Symposium (ONR, Annapolis, MD, 1981), pp. 36–42.
12. R. B. Frey, in 8th International Detonation Symposium (ONR, Albuquerque, NM, 1985), pp. 68–80.
13. N. R. Barton, N. W. Winter, J. E. Reaugh, Model. Simul. 2009, 17, 035003.
14. R. A. Austin, N. R. Barton, J. E. Reaugh, L. E. Fried, J. Appl. Phys. 2015, 117, 18, 185902.
15. MP Kroonblawd, LE Fried, Physical Review Letters 2020, 124 (20), 206002.
16. C. M. Tarver, T. D. Tran, Combustion and Flame, 2004, 137, 1–2, 50-62.
17. C. R. Noble et al. ALE3D: An arbitrary Lagrangian-Eulerian Multi-Physics Code, LLNL-TR-732040, LLNL, 2017.
18. G. A. Levesque, P. A. Vitello, Propellants Explos. Pyrotech. 2015, 40, 303
19. J.J. Dick, D.E. Hooks, R. Menikoff, A.R. Martinez, J. Appl. Phys. 2004, 96 (1), 374.
20. J.E. Reaugh, B.W. White, J.P. Curtis, and Springer, H.K., Propellants Explos. Pyrotech., 2018, 43(7), 703-720.
21. J. G. Bennett, K. S. Haberman, J. N. Johnson, B. W. Asay, Journal of the Mechanics and Physics of Solids, 46:12, 1998, 2303-23.

Question from David Williamson, University of Cambridge
You present on single voids. Will this research be extended to arrays of voids?

Answer from Harry Springer
Yes, that is the plan.

Question from Ericka Amborn, ARA
Have you or do you have plans to compare your simulation results with experimental data?

Answer from Harry Springer
Yes. Experimental validation of the simulation results is an important next step.

Question from Aaron Benfante, US Army
Was any air allowed to escape the cavity during?

Answer from Harry Springer
No, air was not allowed to escape pore during dynamic compression in simulations.

Question from Aaron Benfante, US Army
How prolate and oblate were your spheroids?

Answer from Harry Springer
3:1 aspect ratio of major to minor radii.

Question from Paul Delery, Air Force Armament Directorate
Have you looked at sizes larger than 1mm or plan to see what the effects of larger pore sizes have on heating?

Answer from Harry Springer
Future plans include investigating larger pore sizes to determine if it changes partitioning of heating from plastic/viscous work vs pore gas compression with conduction to adjacent explosive.

Question from Paul Lafourcade, CEA
Would the gas pressure increase during compaction be high enough to open pre-existing cracks from the pore surface? Does ALE3D have such capabilities?

Answer from Harry Springer
Possibly. This may depend on the crack location/size on the pore surface, energetic crystal orientation, how much residual stress/strain is on it after unloading of the applied triangular compression pulse and other factors. The fracture mode (tensile, shear, etc) also needs to be considered. While ALE3D has been used to investigate dynamic fracture problems, I'm not certain it would have the capabilities to capture all the physics and mechanics necessary for this particular problem.